


ARTICLE

<https://doi.org/10.1038/s41467-019-08786-x>

OPEN

Single gametophyte sequencing reveals that crossover events differ between sexes in maize

Cheng Luo¹, Xiang Li¹, Qinghua Zhang¹ & Jianbing Yan ¹

Meiotic crossover (CO) plays a key role in producing gametophytes and generating genetic variation. The patterns of CO production differ inter- and intra-species, as well as between sexes. However, sex-specific patterns of CO production have not been accurately profiled independently of genetic backgrounds in maize. Here, we develop a method to isolate single female gametophyte for genomes sequencing in maize. We show that more COs are observed in male (19.3 per microspore) than in female (12.4 per embryo sac). Based on Beam-Film model, the more designated class I and II COs are identified in male than in female. In addition, CO maturation inefficiency (CMI) is detected in some genetic backgrounds, suggesting that maize may be an ideal model for dissecting CMI. This research provides insights toward understanding the molecular mechanism of CO production between sexes and may help to improve maize breeding efficiency through paternal selection.

¹National Key Laboratory of Crop Genetic Improvement, Huazhong Agricultural University, Wuhan 430070, China. These authors contributed equally: C. Luo, X. Li. Correspondence and requests for materials should be addressed to X.L. (email: lixiang1989@webmail.hzau.edu.cn) or J.Y. (email: yjianbing@mail.hzau.edu.cn)

Meiosis transforms sexual organisms from sporophyte ($2n$) to gametophyte (n) generation. Crossover (CO) is a key event during meiosis, since it not only ensures the success of homologous chromosome separation by chiasmata^{1,2} but also introduces large-scale genetic variation by inter-homolog exchange. CO is produced in a series of highly regulated steps. Briefly, meiotic recombination initiates from double-strand breaks (DSBs) followed by inter-homolog invasion, generating inter-homologous intermediates, which will be resolved to CO or non-crossover (NCO) recombination through different pathways, including double Holliday junction and synthesis-dependent strand annealing^{3–5}. CO frequency, distribution, and interference could differ inter-⁶ and intra-species⁷. Sex differences in CO frequency was discovered first in the 1920s^{8,9}, and has been observed in many species to date¹⁰. In fruit fly¹¹ and silkworm¹², in particular, COs were produced only in male and female meiosis, respectively. Many factors contribute to sex difference in CO production. First, given that synaptonemal complex (SC) length was positively correlated with CO amount^{13,14}, the sex with longer SC harbors more COs, such as female of human¹⁵ and mouse¹⁶. Second, it was reported that 13 variants were identified as candidates to affect recombination rate in the Icelandic human population. Three of them only affect the male recombination rate, and seven of them only affect the female recombination rate¹⁷. These suggested that the sex-specific variants could result in divergence of CO pattern, probably through governing meiotic DSB initiation and repair pathway. Third, selfish elements increase their transmission probability during sex-specific gametogenesis, often disrupting the Mendelian segregation ratio (2:2) in only one sex, like t-haplotype for male in mouse¹⁸ and abnormal chromosome 10 (Ab10) for female in maize^{19,20}.

Diocious species, such as human and mouse, may not be perfect models to estimate sex difference of CO production, since the difference between individuals is derived not only from sexes but also from genetic backgrounds. Hermaphroditic species, like *Arabidopsis* and maize, can produce the gametophytes sharing the same background; in this case, the difference in CO pattern could only result from sex-specific elements. In *Arabidopsis* and maize, genotyping individuals from reciprocal crosses revealed sex differences in CO patterns^{21–23}. Comparison of CO patterns between single sperm and egg^{24,25} in human provides a strategy to evaluate sex differences of recombination pattern during one meiosis. In maize, single microspores were isolated and sequenced to profile the male recombination pattern²⁶. Although the isolation of maize embryo sacs and eggs was reported²⁷, sequencing remains a challenge, owing to the large number of nucellar cells around embryo sac. Here we develop a method to isolate antipodal cells from single embryo sacs for DNA amplification and high-throughput sequencing. The female CO pattern

is profiled in high resolution. Through comparing the CO patterns of embryo sac and microspore populations sharing the same background, sex differences are found, with fewer COs and hot regions in female than male. The 84% difference in CO number is attributed to the difference in the number of CO hot regions between sexes. Based on Beam-Film (BF) model, it is determined that longer interference distance and fewer non-interfering COs (class II COs) are in female, independent of genetic backgrounds. CO maturation inefficiency (CMI) exists in some genetic backgrounds. These results provide insights into the mechanism of sex-specific CO production and toward improving breeding efficiency in maize. Single gametophyte sequencing could be a general strategy to analyze sex-specific recombination among any species.

Results

Isolation of antipodal cells from a single embryo sac. In angiosperm, female gametophyte generation begins at meiosis, which triggers megaspores from a megasporocyte. Micropylar megaspores are degraded, and the chalazal-most megaspore divides producing an embryo sac²⁸. To isolate the female gametophyte, F_1 individuals were planted. Their background (Zheng58 \times SK) was the same as those of the microspore-derived F_1 individuals sequenced previously²⁶. A mass of cells, including embryo sac and nucellar cells, was extracted from the ovule and put into a drop of multiple enzymatic mixture for 15 min. The embryo sac could then be distinguished, separated from nucellar cells using a glass micropipette, and transferred to a clear drop of isotonic buffer. In *Arabidopsis*, one embryo sac contains three antipodal cells; however, dozens of antipodal cells were reported in maize²⁹ (Fig. 1a). These antipodal cells share the same haplotype. To increase the copy number of the original DNA for amplification and sequencing coverage, a few (5–15) antipodal cells were isolated from the same embryo sac for cell lysis and multiple displacement amplification (MDA) of DNA (see Methods; Fig. 1b). The integrity of MDA products was validated using 10 molecular markers as described previously²⁶. The amplified products with at least 8 positive markers could be qualified (Supplementary Figure 1) for sequencing. In total, 106 samples of qualified embryo sac DNA from 14 F_1 individuals were selected for whole-genome sequencing. A total of 3,009,050,118 reads were obtained. On average, 28,215,923 filtered reads per sample could be mapped to and covered \sim 40% of the maize B73 v4 reference genome³⁰ at \sim 1.2 \times depth (Supplementary Data 1). Based on the fine-assembled B73 v4 reference genome and validation results, the invalidated small bins and false-positive COs have been eliminated for further analysis (for details see Methods). To compare CO landscapes between both sexes, the same standard was also applied to the single microspore ($n = 96$)

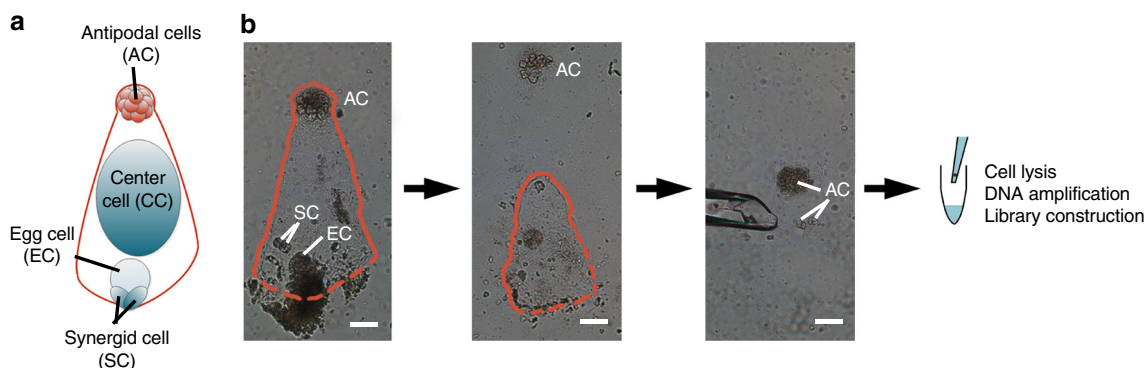


Fig. 1 The microscopic isolation of antipodal cells from maize embryo sac. **a** A diagram of a mature embryo sac. **b** The brief steps of microscopic isolation. The red line profiles embryo sac putatively. Bar = 100 μ m

(~0.29 cM/Mb, total 614.8 cM) is 0.64-fold of CO frequency in male (~0.46 cM/Mb, total 962.5 cM). In human¹⁵ and mouse¹⁶, more COs occur in female than male, which likely results from longer SC length for female. In *Arabidopsis*²¹, female meiosis produces less COs along a shorter SC than male. However, owing to that synaptonemal complex (SC) length of maize female meiosis was hardly captured, sex difference of SC length has not been profiled in maize until now. Additionally, it was also observed that female CO numbers are positively correlated with chromosome length (physical length and male SC length of the inbred line KYS¹⁴) (Supplementary Figure 4), in accord with previous results in male²⁶. CO frequency from the 14 embryo sac donors was relatively stable (Supplementary Figure 5), while the two microspore donors produced different CO amounts²⁶.

Sex-specific CO distribution. The recombination frequency map (cM/Mb) was constructed using 3 Mb windows for each gametophyte population and was compared to the map for recombinant inbred line (RIL) population sharing the same genetic background³¹ (Fig. 2a). To accurately estimate the chromosome-level difference between sexes, position of each CO was divided by chromosome arm length. Both male and female COs were concentrated in peri-telomere with the coincided distribution patterns (Fig. 2b). This was inconsistent within human that male meiosis produces more COs in peri-telomere than female, although COs in both sex were concentrated in peri-telomere³². The gametophyte and RIL populations within the same background share a similar CO distribution pattern (Fig. 2a). It was also reported that different CO distribution patterns were uncovered in populations with different genetic backgrounds⁷. These suggest that genetic background may affect CO distribution, probably through the genome modifications or (and) hot-spot distribution. To further compare the sex-specific CO patterns, CO hot regions were defined as the 3 Mb windows with more than 1 cM/Mb and a total of 123 hot regions were discovered (stars in Fig. 2a, Supplementary Data 4). In female and male, 71 (10.1%) and 112 (15.9%) hot regions contained 755 (57.55%) and 1190 (64.12%) COs, respectively, which suggests that the dramatic difference in CO frequency between sexes was positively correlated by the differing number of hot regions. To further profile difference of hot regions between gametophyte populations, sex-preferred hot regions were defined as greater than twofold CO frequency of the other sex. We observed 11 female-preferred (red stars in Fig. 2a) and 53 male-preferred (yellow stars in Fig. 2a) hot regions. One of the extreme male-specific hot regions is near peri-telomere of chromosome 6, whereas female CO is almost absent. It is suggested that the mechanism of CO hot region determination may differ between sexes.

The intervals between two adjacent bins were defined as CO locations. And 92.6% (1216) and 81.1% (1506) of them could be limited to <200 kb in female and male, respectively, based on B73 v4 reference genome (Supplementary Figure 6). The higher resolution in female may partly be contributed by the higher sequencing coverage and several DNA copies (antipodal cells) for original MDA, while only single copy (single microspore DNA) was initiated in male. The 568 (43.3%) female and 350 (18.9%) male COs located under 10 kb were selected to analyze CO distribution at the gene scale. The relative distance from each CO (median position) to its closest gene was calculated (Fig. 2c). Comparing to five sets of randomly simulated positions, COs concentrate in the translation start sites and translation terminal sites of genes for each sex (Fig. 2c, two-sided Kolmogorov–Smirnov test $P < 2.2 \times 10^{-16}$ for female and male), which is consistent with the previous result based on the B73 v3

reference²⁶. Intragenic enrichment of CO was also observed in yeast³³ and in *Arabidopsis*³⁴, but not in human^{24,25}.

Distinct CO interference patterns in different sexes. CO interference was observed that COs inhibit the production of nearby COs^{35–37}, preventing from CO clusters in each sample, thus increasing the evenness of CO distribution. In some organisms, such as yeast³⁸, *Arabidopsis thaliana*³⁹, maize⁴⁰, and mouse⁴¹, most COs respond to interference, defined as class (type) I COs, produced via ZMM pathway⁵ (relying on Zip1, Zip2, Zip3, Zip4, Mer3, Msh4, and Msh5); whereas, the COs insensitive to interference are defined as class (type) II COs, dependent on Mus81 and Mms4/Eme1 pathway³⁷. To profile CO interference in gametophyte populations, the coefficient of coincidence (CoC) was calculated that double CO rate in pair of intervals was divided by the product of two single CO rates in these intervals (see below), based on genetic distance. The CoC curve was plotted by the mean CoC for each distance between interval pairs. The difference in CoC curves suggests the sex-specific interference pattern and CO formation mechanism (Fig. 3a).

The fluctuant CoC values above 1 were found as a negative interference phenomenon in both sexes' sets, which could be led from the positive interference as discussed in a previous study⁴³. To accurately estimate interference, a mechanism-based CO simulation model, the BF model^{42–44} was used. This model was proposed to quantitatively explain experimental CO pattern datasets in many organisms, such as identifying the reduced interference in *top2* mutant of yeast⁴⁵ and CMI in human female meiosis⁴⁶, suggesting its reliability and robustness. In this model, a stress-and-stress relief mechanism was proposed to explain the formation of CO patterning (Fig. 3b). Briefly, a set of precursors are regularly distributed among and along bivalents. Mechanical stress promotes occurrence of CO designation during inter-homolog interactions. Precursors have varying stress response sensitivities. Average number of precursors was defined as parameter N . As stress is released, the precursor with the highest potential becomes interfering class I CO; then the local stress alleviates around this position, inhibiting the other precursors nearby. The distance that interference signal spreads was defined as parameter L , which reflects interference level. Independent of the process of class I CO designation, non-interfering class II CO could be generated from the precursors not becoming class I CO. The probability of class (type) II CO production was defined as parameter T2prob, which reflects the amount of class II COs. CMI would have happened, blocking some designated COs developing into actual COs. The mature rate of class I COs was defined as parameter M (Fig. 3b). These four main parameters (N , L , T2prob, and M) connecting biological process, critically determines CO pattern in meiosis (see all detailed parameters in Methods).

By determining values of the parameters (Supplementary Table 3), CO patterns could be simulated by the BF model with high repeatability. When simulated and observed CO sets share the fitting (1) CoC curve (along proportion of genetic distance), (2) average number and distribution of COs per bivalent, the parameter values could quantify the production of observed COs. When calculating CoC by using only the class I CO dataset, distance at which $\text{CoC} = 0.5$ ($L_{\text{CoC}=0.5}$) in CoC pattern could evaluate interference level^{43,46}; however, $L_{\text{CoC}=0.5}$ is also affected by class II COs number (T2prob) when calculating CoC (Supplementary Figure 7a). Instead, we found that the distance at which $\text{CoC} = 1$ ($\text{Distance}_{\text{CoC}=1}$) is invariable and the CoC value at minimum distance ($\text{CoC}_{\text{Distance=minimum}}$) increases, when T2prob changes (Supplementary Figure 7b). These suggest that $\text{Distance}_{\text{CoC}=1}$ and $\text{CoC}_{\text{Distance=minimum}}$ directly reflect L and T2prob values, respectively. Through testing a range of parameter

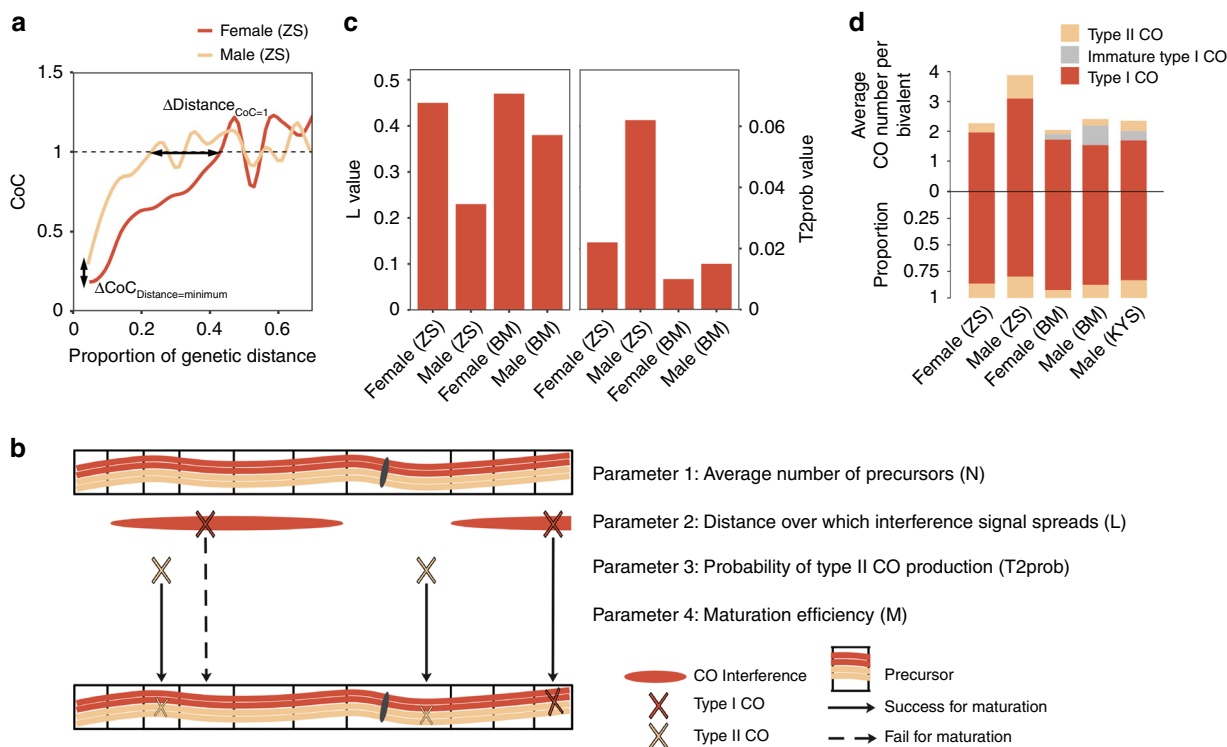


Fig. 3 Features of crossover (CO) interference exhibiting sex difference. **a** The CoC curves for female and male gametophyte populations. $\text{Distance}_{\text{CoC}=1}$ represents the distance at which $\text{CoC} = 1$. $\text{CoC}_{\text{distance=minimum}}$ represents the CoC value at minimum distance. $\Delta\text{Distance}_{\text{CoC}=1}$ and $\Delta\text{CoC}_{\text{distance=minimum}}$ represent the D -value of $\text{Distance}_{\text{CoC}=1}$ and $\text{CoC}_{\text{distance=minimum}}$ between sexes, respectively. **b** A diagram illustrating the Beam-Film model shows the main steps of CO formation and the main parameters for these steps. **c** The values of parameters L and $T2\text{prob}$ in male and female meiosis within different genetic backgrounds. **d** The numbers (upper) and proportion (lower) of type I and II COs were shown. The putative numbers of immature type I COs derived from CMI were also present (gray in upper half of the graph). ZS is short for the F_1 from the cross of inbred lines Zheng58 and SK, profiled by single gametophyte sequencing. BM is short for the F_1 from the cross of inbred lines B73 and Mo17, profiled by sequencing progeny from reciprocal crosses. Source data of Fig. 3a are provided in a Source Data file.

sets, the best-fit values for the two gametophyte populations within the Zheng58 \times SK background were determined ($n = 240$ bivalents for male and $n = 265$ bivalents for female; Supplementary Figure 8). Varying parameters from the best simulation could not provide satisfactory match to the experimental data (Supplementary Figure 9), which indicated that these values of parameters are reliable.

Within the Zheng58 \times SK background, higher $\text{Distance}_{\text{CoC}=1}$ and lower $\text{CoC}_{\text{distance=minimum}}$ on female CoC curve (Fig. 3a) indicates a longer interference distance and less class II CO amounts in female meiosis, respectively. As determined by simulation, L in female (0.45) is 1.96 folds of L in male (0.23), while $T2\text{prob}$ in female (0.022) is 0.35 folds of L in male (0.062) (Fig. 3c). To validate whether the sample sizes were enough to distinguish sex differences of L and $T2\text{prob}$, the bootstrapping analysis was performed by using another CO set observing late recombination nodules of microsporocyte of an inbred line KYS¹⁴ ($n = 2080$ bivalents). After randomly extracting 320 bivalents (in which CO number is equal to CO number in the embryo sac population) for 100 times, CoC curves of these sets were profiled (Supplementary Figure 10a). D -values of the $\text{Distance}_{\text{CoC}=1}$ and $\text{CoC}_{\text{distance=minimum}}$ in each pair of extracted sets were calculated ($\Delta\text{Distance}_{\text{CoC}=1}$ and $\Delta\text{CoC}_{\text{distance=minimum}}$). The D -values between female and male gametophyte sets within the Zheng58 \times SK background were higher than 99.1% and 88.2% of the bootstrapped D -value sets, respectively (Supplementary Figure 10b), suggesting 99.1% and 88.2% confidence. The Zheng58 \times SK COs from chromosomes with similar length were selected to simulate and to compare between sexes (Supplementary

Figure 11). For long chromosomes (chr. 1–5, 135.71–108.19 μm for KYS male SC) and short chromosomes (chr. 6–10, 93.83–77.7 μm), L values were higher in female (0.30 and 0.46) than in male (0.19 and 0.27, respectively). We used higher N in long chromosomes ($N = 18$) than in short chromosomes ($N = 12$), as precursor number positively correlated with SC length. In this case, $T2\text{prob}$ values of these sets in long and short chromosomes equal the values of the set in all chromosomes for both sexes (0.022 for female and 0.062 for male). These approved that the sex difference of parameters L and $T2\text{prob}$, independent of chromosome length. Moreover, based on the BF model, the best-fit parameters of CO sets from reciprocal crossing populations²³ between F_1 (B73 \times Mo17) and B73 ($n = 337.5$ and 305 bivalents when F_1 is taken as the maternal and paternal, respectively) were determined (Supplementary Figure 8). Compared with male meiosis, the higher L and the lower $T2\text{prob}$ of female meiosis were also detected within the B73 \times Mo17 background, which was similar with the Zheng58 \times SK background (Fig. 3c; supplementary Table 3). Additionally, through simulating on a statistical oriented gamma model^{40,47} (Supplementary Figure 12), the stronger interference intensity (higher parameter nu) and less proportion of non-interfering COs (lower parameter p) in female meiosis was still detected within both backgrounds (Supplementary Figure 13). Combining these results, it could be concluded that the sex differences in interference strength and class II CO amounts are present, independent of backgrounds.

It's puzzled that type I CO frequency within B73 \times Mo17 background was higher in female (17.2 for BF and 18.2 for

gamma model) than in male (15.4 for BF and 16.4 for gamma model), detected by using both BF (Fig. 3d) and gamma (Supplementary Figure 13) models; however, interference intensity is stronger in female meiosis than in male. These may only be explained by the unexpected CMI in this background, profiled by BF model. CMI was detected in male ($M = 0.7$) and female ($M = 0.9$) meiosis within the B73 × Mo17 background, as well as in KYS male meiosis ($M = 0.84$). For KYS CO set, at which $M = 1$, simulations always predict too many COs (2.5 COs for simulation and 2.0 COs for observation per bivalent, Supplementary Figure 14a) based on the best-fit CoC curve (Supplementary Figure 14b). In this case under $M = 1$, decreasing the number of active precursor by using highly skewed distribution of precursor sensitivity to CO designation (changing A from 1 to 6), decreased efficiency of precursor formation through DSB progress (changing Y from 1 to 0.5) and decreased average number of precursors per bivalent (changing N from 16 to 9) could reduce simulated COs to the experimental level (~2.0), but the simulated CoC curves would not be best fitted to the observed (Supplementary Figure 14). These three parameters were also not changed in human female meiosis with CMI⁴⁶. For the CO sets within the B73 × Mo17 background, it was also proposed that M does not equal 1. Additionally, the bivalents without chiasmata were also observed in male meiosis of KYS¹⁴, recording with CMI. Combining these sets, CMI indeed exists in B73 × Mo17 and KYS, but not in Zheng58 × SK, suggesting that genetic background is probably key for CMI in maize.

Based on these parameters of BF model, it was calculated that both class I and II CO frequency of female (1.96 and 0.30 per bivalent) are less than that of male (3.10 and 0.78 per bivalent, respectively) within the Zheng58 × SK background (Fig. 3d). Fewer class I and II COs of female meiosis were also reported in *Arabidopsis*⁴⁸. Although class I COs within the B73 × Mo17 background is more in female than in male meiosis based on BF and gamma models (see above), class II COs (0.14) and the designated class I COs (1.91), which are the sum of the mature and immature type I COs owing to CMI, are less in female than in male (0.22 and 2.19, respectively). These imply that COs of female meiosis are less than that of male unless CMI exists in maize. The precursor number (N) usually varies from 4 to 25 folds of chiasmata number in maize male meiosis^{49–51}. We also tried to increase N (from 16 to 18, 20, 22, and 24) to simulate COs, resulting the increased CoC_{Distance=minimum} and the decreased T2prob value (from 0.062 to 0.048, 0.042, 0.038, and 0.034, respectively) (Supplementary Figure 15). However, the number and proportion of class I/class II COs were invariable within these pairs of parameters. Therefore, sex difference of class I and II number could still be concluded, no matter how N value changed.

Discussion

We developed a method to sequence a single female gametophyte genome, through isolating antipodal cells from an embryo sac. This research suggests that sequencing single gametophyte genomes could be a general strategy to profile the sex-specific CO patterns of a single meiosis in other species as well. Analyzing meiotic CO is of fundamental importance for understanding the dynamics of genome evolution. Sex difference in CO pattern was reported in many species¹⁰. Here, under the same background of hermaphroditic species maize, sex differences in CO production could be accurately detected, owing to only caused by sex-specific activation of functional elements. Comparing the two datasets within the Zheng58 × SK background, it is surprising that many more COs were produced in male than in female (19.3 per microspore and 12.4 per embryo sac). This is consistent with the higher number of CO hot regions in male (112) than in female (71). Within the B73 × Mo17 background, although the CO

numbers in male (8.6) meiosis accompanying CMI are slightly lower than in female (9.3), the sum of observed and immature COs derived from CMI is more in male (12.0) than in female (10.2). These suggest that COs in male may be more than in female unless CMI.

BF model is a comprehensive tool to explain the mechanism of CO production along longitudinal chromosome axis^{42–44}. However, it is hard to capture synaptonemal nuclei in maize female meiosis, thus it is hard to detect female CO (chiasmata or MLH1) loci along SC. To compare the sex difference of CO interference, genetic distance was used to simulate for BF model, which could be reliable owing to that both SC length (μm) and genetic length (cM) of the chromosome are positively correlated with CO frequency. Although the different interference metrics (at genetic distance and SC length) may make various values of simulation parameters, the sex difference can still be revealed through comparing parameter values at the same interference metric (genetic distance). A much higher T2prob in male than female was found within the two backgrounds (Fig. 3c), illustrating that more class II COs formed during male meiosis (Fig. 3d). Since high temperature increases CO number through the class I pathway, but not class II pathway^{52–54}, the detected sex difference of class II CO frequency could be independent of environment factors.

Based on the BF model, CMI was assumed as an underlying event during CO formation, which elevates aneuploidy in human female meiosis⁴⁶. Therefore, dissecting the mechanism of CMI could be important for the understanding of CO production process and possible reducing instances of aneuploidy (like human Down's syndrome). However, the molecular mechanism of CMI cannot be analyzed in human, since the functional elements of this female-specific process have yet to be fully understood. In maize, CMI may also contribute to pollen abortion and embryo aneuploidy. CMI was detected within the B73 × Mo17 and KYS backgrounds but not in Zheng58 × SK, suggesting that CMI may be triggered by a few background-specific elements (genes). Therefore, maize could be an ideal model to dissect the genetic foundation of CMI. With the development of a high-throughput method to detect CMI, the mechanism could be dissected further. Since CO number decreased with the presence of CMI (see Results), selecting the lines without CMI could increase the CO frequency thus enhancing the plant breeding efficiency. Moreover, introgression lines containing target regions without CMI could be used as males in backcross conversions, harboring more COs, especial class II COs, which would result in smaller recombination events in one generation.

The molecular mechanism of sex-specific CO production needs to be analyzed further. In this study, it was observed that SC length is positively related to CO number in both sexes. Nevertheless, nucleosome density, histone variant or modification (H2A.Z, H3K4me3, and H3K9me2), and DNA methylation level^{55,56} at synaptonemal were reported to influence DSB distribution and CO formation largely. Therefore, further analyzing the linkage between these molecular features and BF model parameters could deepen our knowledge of the mechanism of CO production.

Methods

Isolation of antipodal cells from single embryo sac. F₁ individuals from a cross between Zheng58 and SK were planted in Wuhan, China. Ears with more than 15 cm silk were harvested and individual ovules were dissected out. The nucellus was isolated under stereoscope and mixed with a drop containing 1.5% pectinase (Sigma, Darmstadt, Germany), 0.5% pectolyase Y23 (Yakult, Tokyo, Japan), 1% cellulase RS (Yakult, Tokyo, Japan), 1% hemicellulase (Sigma, Darmstadt, Germany), and 0.54 M mannitol. Following 15–20 min incubation, the embryo sac was dissociated from the nucellus and was placed into a drop of 0.54 M mannitol by micropipette. A mass of antipodal cells was observed as cup structure at the chalazal end (Fig. 1), and could be cut off from embryo sac. Then, 5–15 antipodal cells were transferred into one PCR tube containing phosphate-buffered saline buffer

from the REPLI-g Single Cell Kit (Qiagen, Hilden, Germany), and also can be stored at -80°C for a long time for further use.

Whole-genome amplification and sequencing. Based on the standard protocol of REPLI-g Single Cell Kit (Qiagen, Hilden, Germany), lysis of female gametophytes and amplification of whole genome (using MDA) was performed. To validate quality of MDA products, 10 markers differing between parents from 10 chromosomes (1 marker per 1 chromosome) were selected for PCR analysis (Supplementary Figure 1; see primers in Supplementary Table 4). The non-heterozygous markers should be present in haploid gametophytes. In total, 106 products, containing at least 8 qualified markers, were selected for library preparation using KAPA HyperPlus Library Preparation (Kapa Biosystems, Wilmington, MA). After sequencing on Illumina HiSeq 3000 platform in pair-end, 3.1 billion raw reads were obtained for next step of analysis.

SNP calling and filtering. To obtain parental SNPs, sequencing data for parental inbred lines Zheng58⁵⁷ and SK²⁶ were downloaded. Reads were filtered by Trimmomatic⁵⁸, then mapped to maize B73 AGPv4 genome³⁰ by bwa⁵⁹. The uniquely mapped reads were selected for calling SNPs, conducted by samtools⁶⁰ and GATK⁶¹. Parental SNP filtration was according to the following criteria: (1) MAPQ ≥ 10 ; (2) SNPQ ≥ 30 ; (3) $3 \leq \text{DP} \leq 100$ for SK and $4 \leq \text{DP} \leq 200$ for Zheng58; (4) QD ≥ 2 ; (5) FS ≥ 20 ; (6) only homozygous SNPs were retained; and (7) distance between adjacent SNPs is more than 4 bp.

The sequencing data of embryo sacs and microspores sharing the same background²⁶ were filtered by Trimmomatic⁵⁸ and mapped to maize B73 AGPv4 genome³⁰ by using bwa⁵⁹. SNPs were called by samtools⁶⁰, and filtered according to the following criteria: (1) homozygous SNPs; (2) SNPQ ≥ 20 ; (3) SNPs with minor allele frequency > 0.1 ; (4) SNPs can be detected in at least 10 samples; and (5) for each bin, at least 20 adjacent SNPs sharing the same parental background were required.

Short bin validation. In this study, 20 short bins were identified totally (< 1.5 Mb) in female gametophyte population. And we also re-mapped all the reads of male gametophyte population²⁶ on the B73 v4 reference³⁰ and there were 8 bins (all < 1.5 Mb) identified in B73 v4 but not in B73 v3 reference. All the 28 bins were chosen for further validation since double COs in small regions are rare^{7,31}. Based on sanger sequencing, it would be validated if the parental haplotypes and progenies haplotypes are as expected from Illumina sequencing. However, considering the complex maize genome, not all the designed primers can be amplified and sequenced successfully in both parents and progenies. Finally, 9 of 20 female short bins and 3 of 8 male short bins were validated as positive; 3 of 20 female short bins and 1 of 8 male short bins were validated as false positive; and others cannot be validated as positive or false positive due to technical issue. The invalidated and false positive short bins have been eliminated for further analysis. For each bin, the detail results and primer sequences could be found in Supplementary Tables 2 and 4.

CO simulation by using BF model. The BF model mathematically simulates the biological processes of CO production. Parameters in this model could be divided into three classes⁴⁶. The first class determines the array of active precursors, including: (1) N , average number of precursors per bivalent; (2) E , precursor spacing along bivalent; (3) B , precursor distribution in population; (4) Y , efficiency of active precursor formation from DSB; and (5) A , distribution of sensitivity among different precursors. The second class describes the patterning of (interfering) CO designation, including: (1) S_{max} , starting stress level relative to sensitivities of precursors; and (2) L , distance over which interference signal spreads. The third class describes the post-patterning process, including: (1) M , probability of that CO-designated interactions will successfully develop to mature COs; and (2) $T2_{\text{prob}}$, probability of that CO-failed precursors will eventually progress to type II COs.

The SC length is not available in female of maize, but the genetic distance determined by using QTL IciMapping⁶² was used for CoC curve fitting, owing to that both SC and genetic distance are positively correlated with CO number. In the CoC curves of both sexes against absolute genetic distance (Supplementary Figure 16), similar $\text{Distance}_{\text{CoC}=1}$ values were observed, which is consistent with the result in the curves against SC length²⁵. Through determining the values of the parameters by many times of trial and error, best-fit predictions can be generally approached. However, the simulated COs are at the bivalent level, while the experimental is at the chromatid level. Therefore, CO array exported from BF model simulation needs to be transformed to the chromatid level. In detail, one CO in bivalent could happen in four pairs between each two chromatids, with the same probability (25% for each pair) (Supplementary Figure 17a); consequently, these pairs for all COs in whole bivalent were randomly combined to generate CO sets at the chromatid level, based on binomial distribution. The simulated (bivalent level) and transformed (chromatid level) CO sets, as well as the observed CO sets of tetrad and microspore level, share the same $\text{Distance}_{\text{CoC}=1}$ value and $\text{CoC}_{\text{Distance}=\text{minimum}}$ value (Supplementary Figure 17b). Owing to the large sample size ($n = 5000$), the CoC curves of simulated and transformed sets almost coincide. In addition, the average number and distribution of CO in simulated (bivalent level) and transformed (chromatid level) sets correspond to those in tetrad

(bivalent level) and microspore (chromatid level) set, respectively (Supplementary Figure 17c). These suggest that the transformation is reliable and accurate.

CO simulation by using gamma model. Gamma model mathematically described the distribution of inter-CO distance, estimating interference strength using parameter nu . Parameter p was defined as the proportion of non-interfering COs^{40,63}. Simulating inter-CO distance distribution using gamma model was conducted by CO distribution analyzer (CODA) software⁶⁴ (version 1.1), following the manual. We set simulation number at 5000 and used maximum likelihood method to obtain the best-fit inter-CO distance distributions.

Code availability. BF model analysis was conducted by previously published MATLAB program, which is available at https://projects.iq.harvard.edu/kleckner_lab/lab-software.

Reporting summary. Further information on experimental design is available in the Nature Research Reporting Summary linked to this article.

Data availability

Data supporting the findings of this work are available within the paper and its Supplementary Information files and from the corresponding authors upon reasonable request. The sequencing dataset for single gametophyte genomes were deposited in the NCBI BioProject under accession code PRJNA489007. The source data underlying Fig. 3a and Supplementary Figures 1, 7, 8, 9, 10, 11, 15a, 16, and 17 are provided as a Source Data file.

Received: 14 September 2018 Accepted: 24 January 2019

Published online: 15 February 2019

References

- Kleckner, N. Meiosis: how could it work? *Proc. Natl Acad. Sci. USA* **93**, 8167–8174 (1996).
- Otto, S. P. & Barton, N. H. The evolution of recombination: removing the limits to natural selection. *Genetics* **147**, 879–906 (1997).
- Holliday, R. A mechanism for gene conversion in fungi. *Genet. Res.* **5**, 282–304 (1964).
- Allers, T. & Lichten, M. Differential timing and control of noncrossover and crossover recombination during meiosis. *Cell* **106**, 47–57 (2001).
- Mercier, R., Mézard, C., Jenczewski, E., Macaisne, N. & Grelon, M. The molecular biology of meiosis in plants. *Annu. Rev. Plant Biol.* **66**, 297–327 (2015).
- Smukowski, C. S. & Noor, M. A. F. Recombination rate variation in closely related species. *Heredity* **107**, 496–508 (2011).
- Bauer, E. et al. Intraspecific variation of recombination rate in maize. *Genome Biol.* **14**, R103 (2013).
- Haldane, J. B. S. Sex ratio and unisexual sterility in hybrid animals. *J. Genet.* **12**, 101–109 (1922).
- Huxley, J. S. Sexual difference of linkage in *Gammarus chevreuxi*. *J. Genet.* **20**, 145–156 (1928).
- Brandvain, Y. & Coop, G. Scrambling eggs: meiotic drive and the evolution of female recombination rates. *Genetics* **190**, 709–723 (2012).
- Cladera, J. L. Absence of recombination in the male of *Ceratitidis capitata*. *Experientia* **37**, 342–343 (1981).
- Goldsmith, M. R. in *Molecular Model Systems in the Lepidoptera* (eds Goldsmith, M. R. & Wilkins, A. S.) 21–76 (Cambridge Univ. Press, New York, 1995).
- Lynn, A. et al. Covariation of synaptonemal complex length and mammalian meiotic exchange rates. *Science* **296**, 2222–2225 (2002).
- Anderson, L. K. et al. High-resolution crossover maps for each bivalent of *Zea mays* using recombination nodules. *Genetics* **165**, 849–865 (2003).
- Kleckner, N., Storlazzi, A. & Zickler, D. Coordinate variation in meiotic pachytene SC length and total crossover/chiasma frequency under conditions of constant DNA length. *Trends Genet.* **19**, 623–628 (2003).
- de Boer, E., Stam, P., Dietrich, A. J., Pastink, A. & Heyting, C. Two levels of interference in mouse meiotic recombination. *Proc. Natl Acad. Sci. USA* **103**, 9607–9612 (2006).
- Kong, A. et al. Common and low-frequency variants associated with genome-wide recombination rate. *Nat. Genet.* **46**, 11–16 (2014).
- Silver, L. M. Mouse tau Haplotypes. *Annu. Rev. Genet.* **19**, 179–208 (1985).
- Rhoades, M. M. Preferential segregation in maize. *Genetics* **27**, 395–407 (1942).
- Dawe, R. K. et al. A Kinesin-14 motor activates neocentromeres to promote meiotic drive in maize. *Cell* **173**, 839–850 (2018).
- Drouaud, J. et al. Sex-specific crossover distributions and variations in interference level along *Arabidopsis thaliana* chromosome 4. *PLoS Genet.* **3**, e106 (2007).
- Giraut, L. et al. Genome-wide crossover distribution in *Arabidopsis thaliana* meiosis reveals sex-specific patterns along chromosomes. *PLoS Genet.* **7**, e1002354 (2011).

23. Kianian, P. M. A. et al. High-resolution crossover mapping reveals similarities and differences of male and female recombination in maize. *Nat. Commun.* **9**, 2370–2379 (2018).
24. Lu, S. et al. Probing meiotic recombination and aneuploidy of single sperm cells by whole-genome sequencing. *Science* **338**, 1627–1630 (2012).
25. Hou, Y. et al. Genome analyses of single human oocytes. *Cell* **155**, 1492–1506 (2013).
26. Li, X., Li, L. & Yan, J. B. Dissecting meiotic recombination based on tetrad analysis by single-microspore sequencing in maize. *Nat. Commun.* **6**, 6648–6656 (2015).
27. Kranz, E., Bautor, J. & Lörz, H. In vitro fertilization of single, isolated gametes of maize mediated by electrofusion. *Sex. Plant Reprod.* **4**, 12–16 (1991).
28. Yang, W. C., Shi, D. Q. & Chen, Y. H. Female gametophyte development in flowering plants. *Rev. Plant Biol.* **61**, 89–108 (2010).
29. Huang, B. Q. & Sheridan, W. F. Female gametophyte development in maize: microtubular organization and embryo sac polarity. *Plant Cell* **6**, 845–861 (1994).
30. Jiao, Y. et al. Improved maize reference genome with single-molecule technologies. *Nature* **546**, 524–527 (2017).
31. Pan, Q. et al. Genome-wide recombination dynamics are associated with phenotypic variation in maize. *New Phytol.* **210**, 1083–1094 (2016).
32. Kong, A. et al. Fine-scale recombination rate differences between sexes, populations and individuals. *Nature* **467**, 1099–1103 (2010).
33. Pan, J. et al. A hierarchical combination of factors shapes the genome-wide topography of yeast meiotic recombination initiation. *Cell* **144**, 719–731 (2011).
34. Wijner, E. et al. The genomic landscape of meiotic crossovers and gene conversions in *Arabidopsis thaliana*. *eLife* **2**, e01426 (2013).
35. Sturtevant, A. H. The behavior of the chromosomes as studied through linkage. *Z. für Indukt. Abstamm. Vererb.* **13**, 234–287 (1915).
36. Muller, H. J. The mechanism of crossing-over. *Am. Nat.* **50**, 193–221 (1916).
37. Mezard, C., Jahns, M. T. & Grelon, M. Where to cross? New insights into the location of meiotic crossovers. *Trends Genet.* **31**, 393–401 (2015).
38. Hollingsworth, N. M. & Brill, S. J. The Mus81 solution to resolution: generating meiotic crossovers without Holliday junctions. *Genes Dev.* **18**, 117–125 (2004).
39. Higgins, J. D., Armstrong, S. J., Franklin, F. C. H. & Jones, G. H. The *Arabidopsis* MutS homolog *AtMSH4* functions at an early step in recombination: evidence for two classes of recombination in *Arabidopsis*. *Genes Dev.* **18**, 2557–2570 (2004).
40. Falque, M., Anderson, L. K., Stack, S. M., Gauthier, F. & Martin, O. C. Two types of meiotic crossovers coexist in maize. *Plant Cell* **21**, 3915–3925 (2009).
41. Guillon, H., Baudat, F., Grey, C., Liskay, R. M. & De Massy, B. Crossover and noncrossover pathways in mouse meiosis. *Mol. Cell* **20**, 563–573 (2005).
42. Kleckner, N. et al. A mechanical basis for chromosome function. *Proc. Natl Acad. Sci. USA* **101**, 12592–12597 (2004).
43. Zhang, L., Liang, Z., Hutchinson, J. & Kleckner, N. Crossover patterning by the beam-film model: analysis and implications. *PLoS Genet.* **10**, e1004042 (2014).
44. White, M. A., Wang, S., Zhang, L. & Kleckner, N. in *Meiosis* (ed Stuart, D. T.) Ch. 18 (Humana Press, New York, 2017).
45. Zhang, L. et al. Topoisomerase II mediates meiotic crossover interference. *Nature* **511**, 551–556 (2014).
46. Wang, S. et al. Inefficient crossover maturation underlies elevated aneuploidy in human female meiosis. *Cell* **168**, 977–989 (2017).
47. McPeck, M. S. & Speed, T. P. Modeling interference in genetic recombination. *Genetics* **139**, 1031–1044 (1995).
48. Basu-Roy, S. et al. Hot regions of non-interfering crossovers coexist with a non-uniformly interfering pathway in *Arabidopsis thaliana*. *Genetics* **165**, 769–779 (2013).
49. Franklin, A. E. et al. Three-dimensional microscopy of the Rad51 recombination protein during meiotic prophase. *Plant Cell* **11**, 809–824 (1999).
50. Stack, S. M. & Anderson, L. K. Crossing over as assessed by late recombination nodules is related to the pattern of synapsis and the distribution of early recombination nodules in maize. *Chromosome Res.* **10**, 329–345 (2002).
51. Sidhu, G. K. et al. Recombination patterns in maize reveal limits to crossover homeostasis. *Proc. Natl Acad. Sci. USA* **112**, 15982–15987 (2015).
52. Francis, K. E. et al. Pollen tetrad-based visual assay for meiotic recombination in *Arabidopsis*. *Proc. Natl Acad. Sci. USA* **104**, 3913–3918 (2007).
53. Lloyd, A., Morgan, C., Franklin, C. & Bomblies, K. Plasticity of meiotic recombination rates in response to temperature in *Arabidopsis*. *Genetics* **208**, 1409–1420 (2018).
54. Modliszewski, J. L. et al. Elevated temperature increases meiotic crossover frequency via the interfering (type I) pathway in *Arabidopsis thaliana*. *PLoS Genet.* **14**, e1007384 (2018).
55. Choi, K. et al. *Arabidopsis* meiotic crossover hot spots overlap with H2A. Z nucleosomes at gene promoters. *Nat. Genet.* **45**, 1327–1336 (2013).
56. Underwood, C. J. et al. Epigenetic activation of meiotic recombination near *Arabidopsis thaliana* centromeres via loss of H3K9me2 and non-CG DNA methylation. *Genome Res.* **28**, 519–531 (2018).
57. Jiao, Y. et al. Genome-wide genetic changes during modern breeding of maize. *Nat. Genet.* **44**, 812–815 (2012).
58. Bolger, A. M., Lohse, M. & Usadel, B. Trimmomatic: a flexible trimmer for Illumina sequence data. *Bioinformatics* **30**, 2114–2120 (2014).
59. Li, H. & Durbin, R. Fast and accurate short read alignment with Burrows–Wheeler transform. *Bioinformatics* **25**, 1754–1760 (2009).
60. Li, H. et al. The sequence alignment/map format and SAMtools. *Bioinformatics* **25**, 2078–2079 (2009).
61. Van der Auwera, G. A. et al. From FastQ data to high-confidence variant calls: the genome analysis toolkit best practices pipeline. *Curr. Protoc. Bioinformatics* **43**, 11.10.1–11.10.33 (2013).
62. Meng, L., Li, H., Zhang, L. & Wang, J. QTL IciMapping: integrated software for genetic linkage map construction and quantitative trait locus mapping in biparental populations. *Crop J.* **3**, 269–283 (2015).
63. Copenhaver, G. P., Housworth, E. A. & Stahl, F. W. Crossover interference in *Arabidopsis*. *Genetics* **160**, 1631–1639 (2002).
64. Gauthier, F., Martin, O. C. & Falque, M. CODA (crossover distribution analyzer): quantitative characterization of crossover position patterns along chromosomes. *BMC Bioinformatics* **12**, 27 (2011).

Acknowledgements

We thank Dr. Anderson, Dr. Matthieu Falque, and Dr. Olivier Martin for providing the CO set of KYS line and CODA software, and thank Dr. Liangran Zhang for the helpful comments about BF model simulation. This research was supported by the National Natural Science Foundation of China (31730064 and 31801125), the National Key Research and Development Program of China (2016YFD0101003), the Hubei Provincial Natural Science Foundation of China (2015CFA008), the National Postdoctoral Program for Innovative Talents (BX201700091), China Postdoctoral Science Foundation (2017M620325), and Huazhong Agricultural University Scientific & Technological Self-Innovation Foundation.

Author contributions

J.Y. and X.L. designed and supervised this study. C.L. isolated single embryo sacs. C.L. and Q.Z. performed the sequencing-associated experiments. C.L. and X.L. analyzed the sequencing data. C.L. performed the BF model simulation. C.L., X.L. and J.Y. prepared the manuscript.

Additional information

Supplementary Information accompanies this paper at <https://doi.org/10.1038/s41467-019-08786-x>.

Competing interests: The authors declare no competing interests.

Reprints and permission information is available online at <http://npg.nature.com/reprintsandpermissions/>

Journal Peer Review Information: *Nature Communications* thanks Christine Mézard, and other anonymous reviewer(s) for their contribution to the peer review of this work.

Publisher's note: Springer Nature remains neutral with regard to jurisdictional claims in published maps and institutional affiliations.



Open Access This article is licensed under a Creative Commons Attribution 4.0 International License, which permits use, sharing, adaptation, distribution and reproduction in any medium or format, as long as you give appropriate credit to the original author(s) and the source, provide a link to the Creative Commons license, and indicate if changes were made. The images or other third party material in this article are included in the article's Creative Commons license, unless indicated otherwise in a credit line to the material. If material is not included in the article's Creative Commons license and your intended use is not permitted by statutory regulation or exceeds the permitted use, you will need to obtain permission directly from the copyright holder. To view a copy of this license, visit <http://creativecommons.org/licenses/by/4.0/>.

© The Author(s) 2019